

Antioxidant Carbon Particles Improve Cerebrovascular Dysfunction

Following Traumatic Brain Injury—Supporting Information

*Brittany R. Bitner^{1,2,¶}, Daniela C. Marcano^{3,4,¶}, Jacob M. Berlin^{3,4,¶,‡}, Roderic H. Fabian^{5,6},
Leela Cherian⁵, James C. Culver², Mary E. Dickinson^{1,2}, Claudia S. Robertson⁵, Robia G.
Pautler^{1,2}, Thomas A. Kent^{1,6,7,*}, and James M. Tour^{3,4,*}*

¹Interdepartmental Program in Translational Biology and Molecular Medicine, and ²Department of Molecular Physiology and Biophysics, Baylor College of Medicine, One Baylor Plaza, Houston, Texas, 77030, USA; ³Department of Chemistry and the ⁴Smalley Institute for Nanoscale Science and Technology, Rice University, MS-222, 6100 Main Street, Houston, Texas 77005, USA; ⁵Department of Neurosurgery and ⁶Department of Neurology, Baylor College of Medicine, One Baylor Plaza, Houston, Texas, 77030, USA; the ⁷Michael E. DeBakey VA Medical Center, 2002 Holcombe Blvd, Houston, Texas 77030, USA. [‡]Present address: Department of Molecular Medicine, The Beckman Research Institute of the City of Hope, Duarte, California, USA.

[¶]These authors contributed equally.

Table of Contents

Figure S1, Images of mock, PEG and PEG-HCC-treated b.End.3 cells, page S2
Figure S2, High resolution images of PEG-HCC-treated and PEG b.End.3 cells, page S3
Figure S3, Fine optical sectioning and orthogonal rendering of z-stacks to differentiate cytoplasm from the cell membrane staining, page S4
Figure S4, DAF-2DA intensity in bEnd.3 cells, page S5
Figure S5, Controls for intracellular SO assay, page S6
Figure S6, Histological and behavioral evidence, page S7-S8
Figure S7, MAP for rats undergoing sham surgery, page S9
Figure S8, Characterization of the PEG-HCCs, page S10
Table S1, TBI impact characteristics, page S10
Table S2, Arterial blood gases, page S11

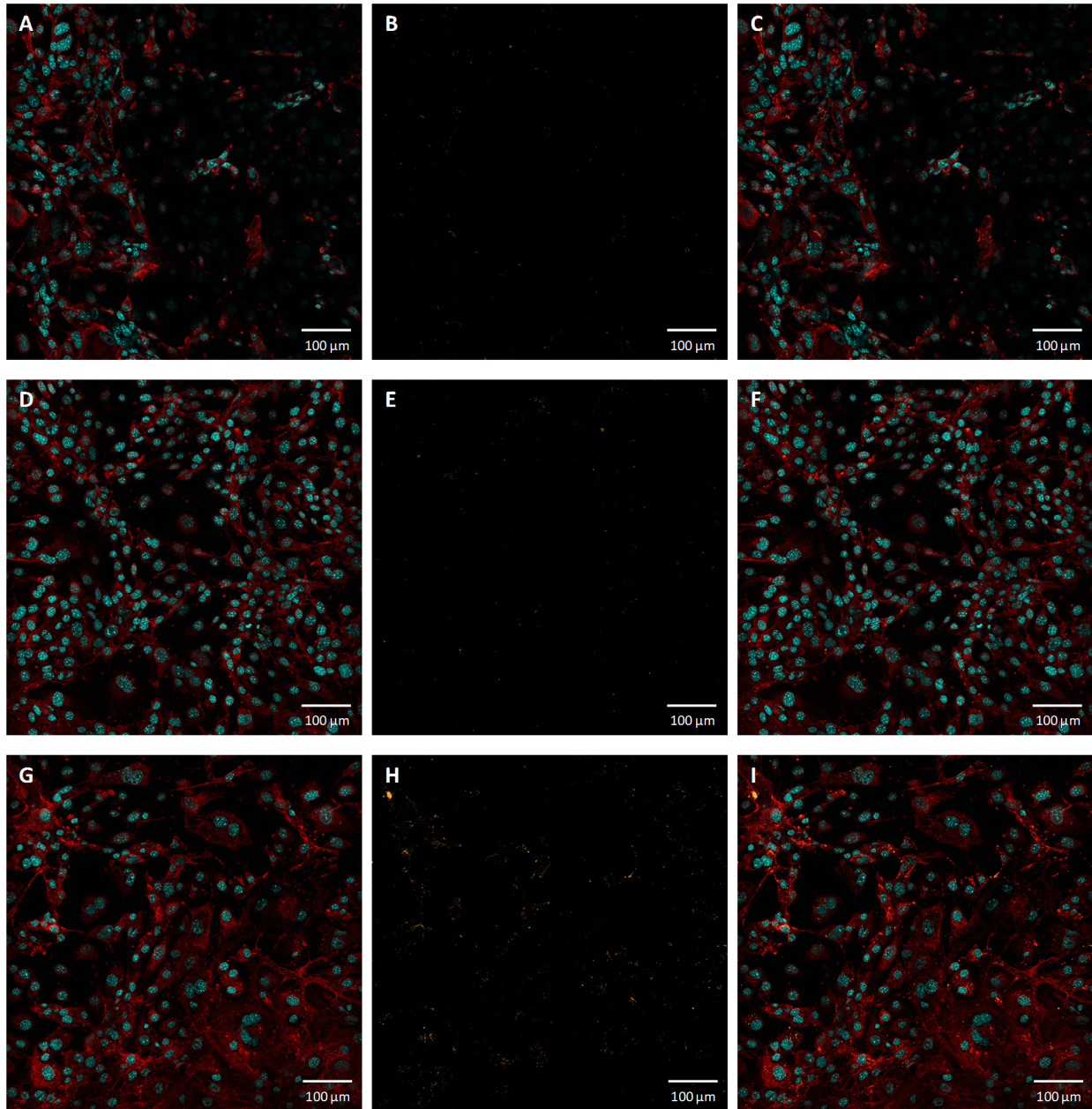


Figure S1. Images of mock, PEG and PEG-HCC-treated b.End.3 cells. Cell nuclei were stained with DAPI (blue), cell membranes with Wheat Germ Agglutinin 594 (red), and PEG and PEG-HCCs were stained using a primary antibody against PEG with an Alexa-633 conjugated secondary antibody (orange). Each set of images was taken with the same settings on a Zeiss LSM 510 confocal microscope, and are shown at the same brightness/contrast levels. (A) The membrane and nuclei stained cells, (B) PEG-stained, and (C) the overlapped images of the mock

treated cells. (D) The membrane and nuclei stained cells, (E) PEG-stained, and (F) overlapped images of the PEG-treated cells. (G) The membrane and nuclei stained cells, (H) PEG-stained, and (I) overlapped images of the PEG-HCC-treated cells. When PEG-HCC-treated cells were stained with the secondary antibody only, no signal was observed indicating that there is no non-specific antibody staining.

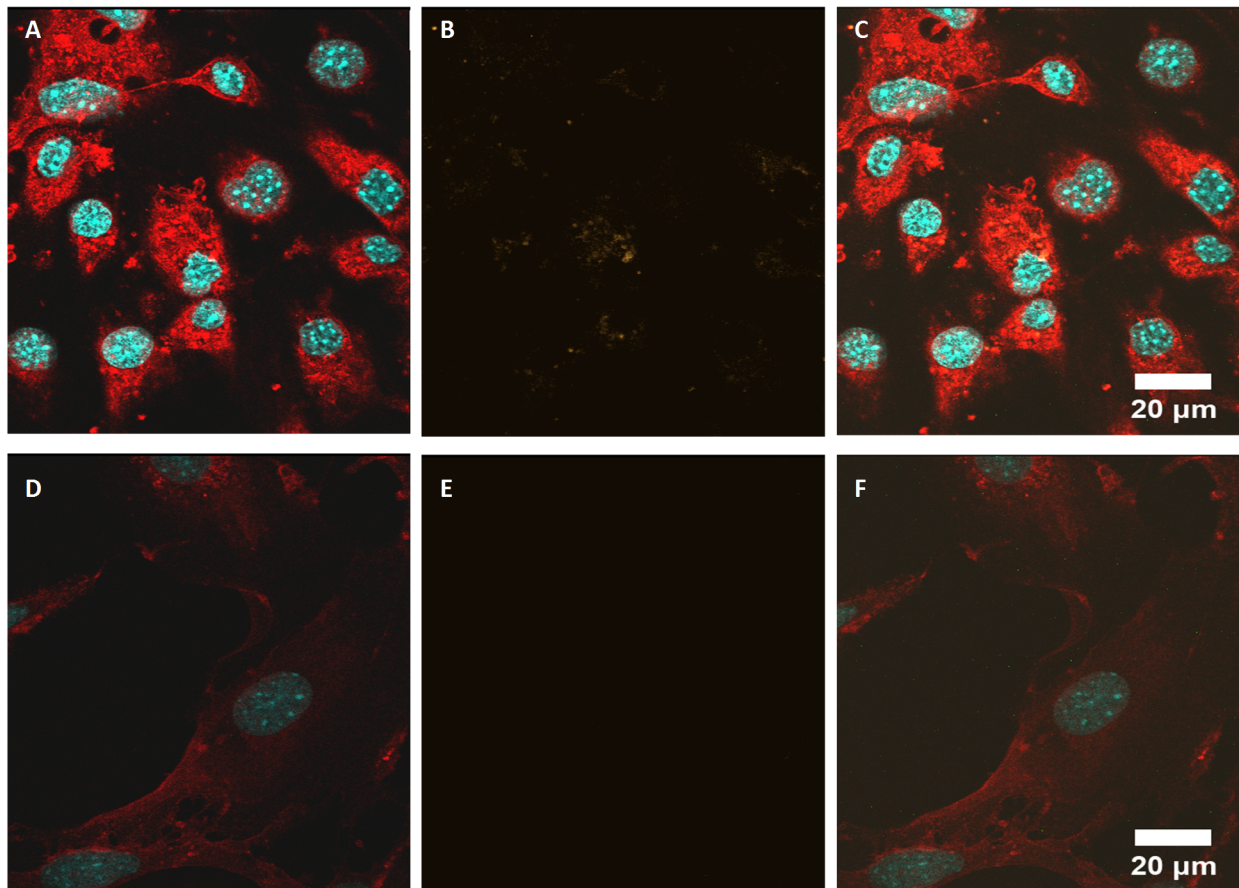


Figure S2. High resolution images of PEG-HCC-treated and PEG b.End.3 cells. Cell nuclei were stained with DAPI (blue), cell membranes with Wheat Germ Agglutinin 594 (red), and PEG and PEG-HCCs were stained using a primary antibody against PEG with an Alexa-633 conjugated secondary antibody (orange). Each set of images were taken with the same settings on a Zeiss LSM 510 confocal microscope, and are shown at the same brightness/contrast levels. (A) The

membrane and nuclei-stained cells, (B) PEG-stained, and (C) overlapped images of the PEG-HCC-treated cells. (D) The membrane and nuclei stained cells, (E) PEG-stained, and (F) overlapped images of the PEG-treated cells.

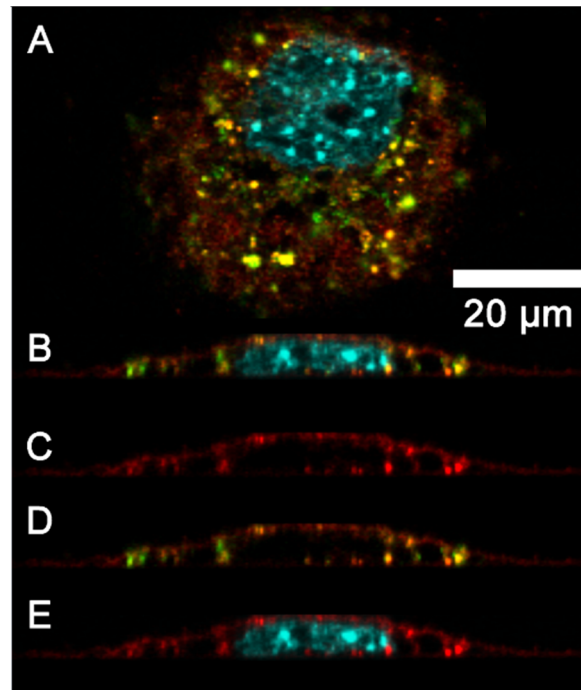
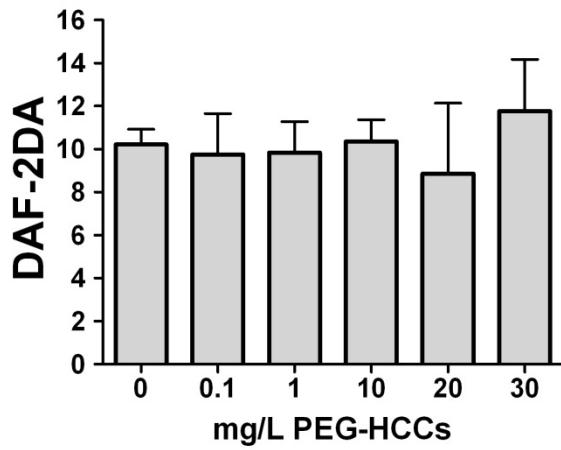


Figure S3. Fine optical sectioning and orthogonal rendering of z-stacks is required in order to resolve the cytoplasm from the cell membrane, which is stained with Wheat Germ Agglutinin (WGA) 594 (red). Shown in (A) is a section through a cell stained with WGA (red), DAPI (blue), and an antibody against PEG to visualize the internalized PEG-HCCs (green). Panels (B) through (E) show an orthogonal slice through the same cell shown in (A), with the following stains: (B) WGA (red), DAPI (blue), and PEG (green); (C) WGA (red); (D) WGA (red) and PEG (green); (E) WGA (red) and DAPI (blue). Visualizing the cell in this way verifies that the WGA staining is specific to the membrane, and that the PEG-HCCs are located intracellularly.

A.



B.

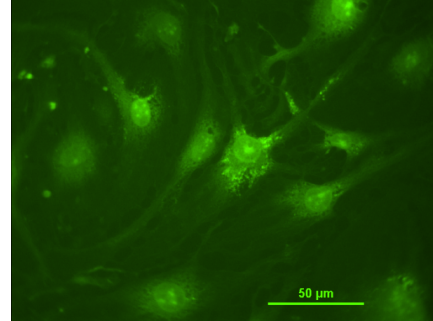


Figure S4. DAF-2DA intensity in bEnd.3 cells that spontaneously generate NO after treatment with increasing concentrations of PEG-HCCs. DAF-2DA is a NO sensitive dye. (A) Concentrations of PEG-HCCs up to 30 mg/L did not quench NO dye fluorescence ($p > .05$ for all comparisons). (B) Fluorescent microscope image of bEnd.3 cells with DAF-2DA. Error bars are s.e.m. Scale bar is 50 μm . Statistics are described in Supplementary Methods section.

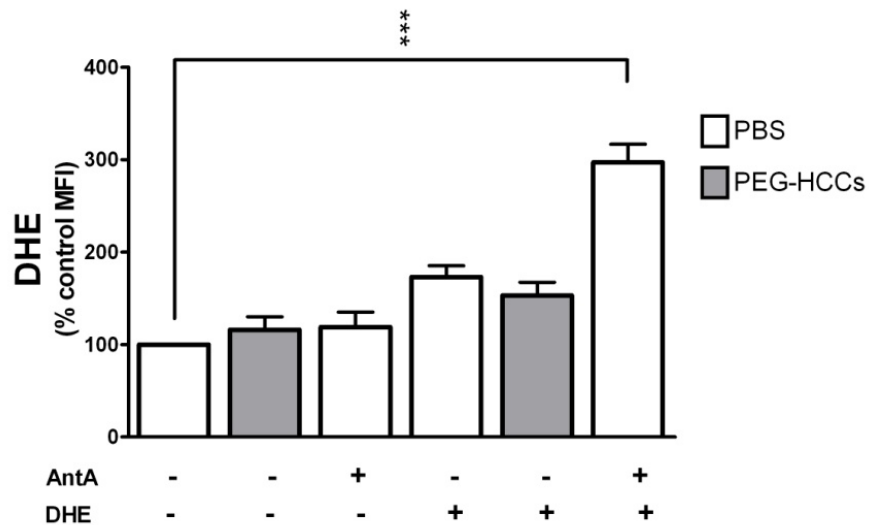
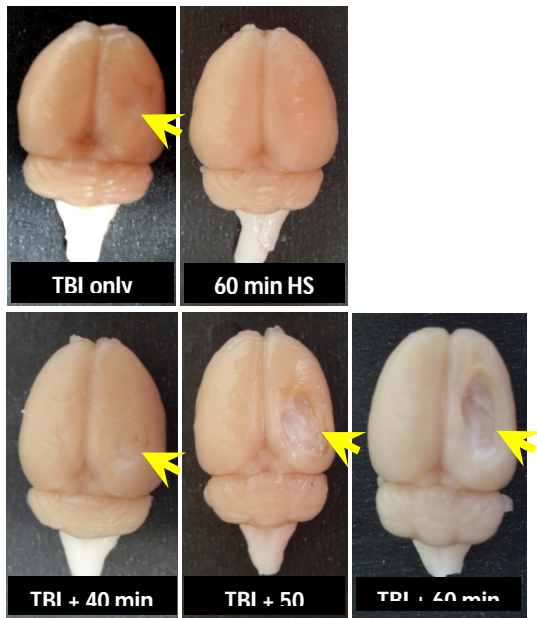
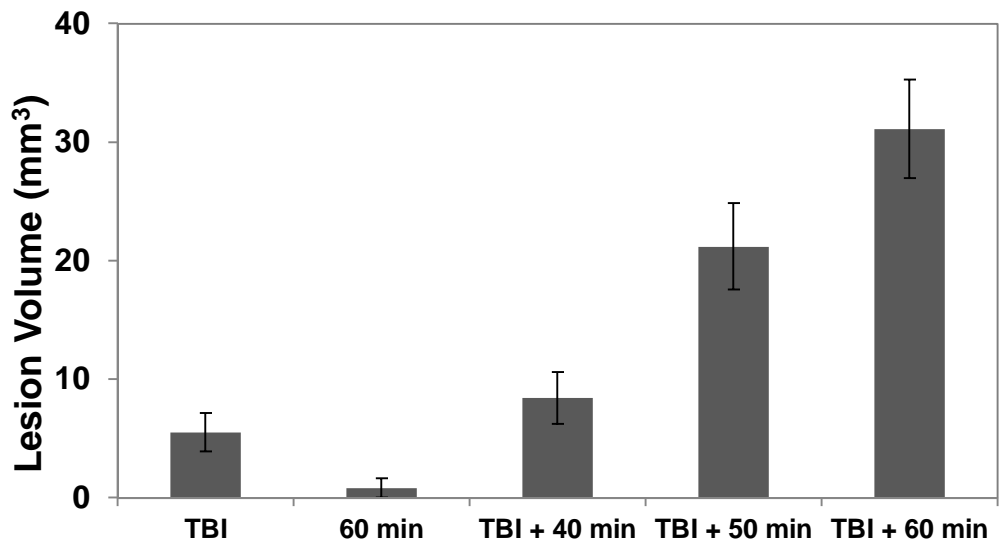


Figure S5. Controls for intracellular SO assay to determine whether there is direct interference between the PEG-HCCs and the fluorescent assay. Cells were treated with or without antimycin A (a mitochondrial toxin that induces SO production). PEG-HCCs were added 15 min later (grey bars) followed by DHE (SO-specific dye) where indicated by +. There was no reduction in either non-specific fluorescence (first three bars) or background fluorescence after addition of DHE (bars 4 and 5). The last combination (bar 6), DHE and antimycin A-treated cells demonstrated, as expected, a significantly higher DHE staining compared to the untreated control (first bar). Statistics are the same as Figure 2 and error bars are s.e.m. Means are the results of a minimum of 5 separate experiments.

A.



B.



C.

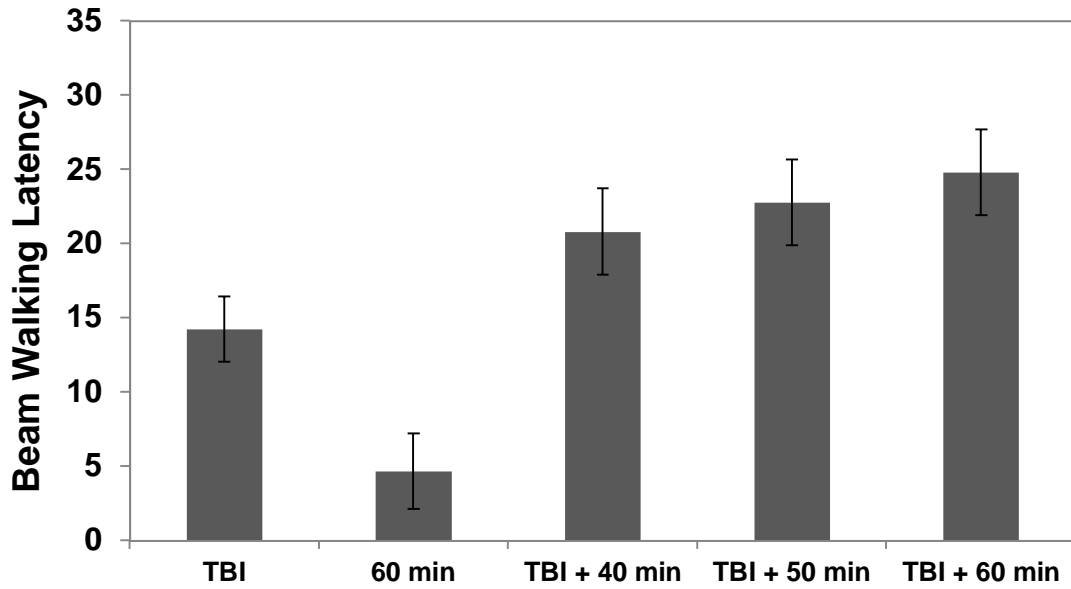


Figure S6. Histological and behavioral evidence that the combination of TBI and hypotension worsens outcome. (A, B) The large change in lesion volume (noted with yellow arrows in A) if TBI is associated with hypotension for 40, 50 and 60 min; recorded 14 days post TBI/hypotension. (C) The decline of behavioral abilities tracks with increased duration of hypotension. Reproduced from ref 30 of main paper.

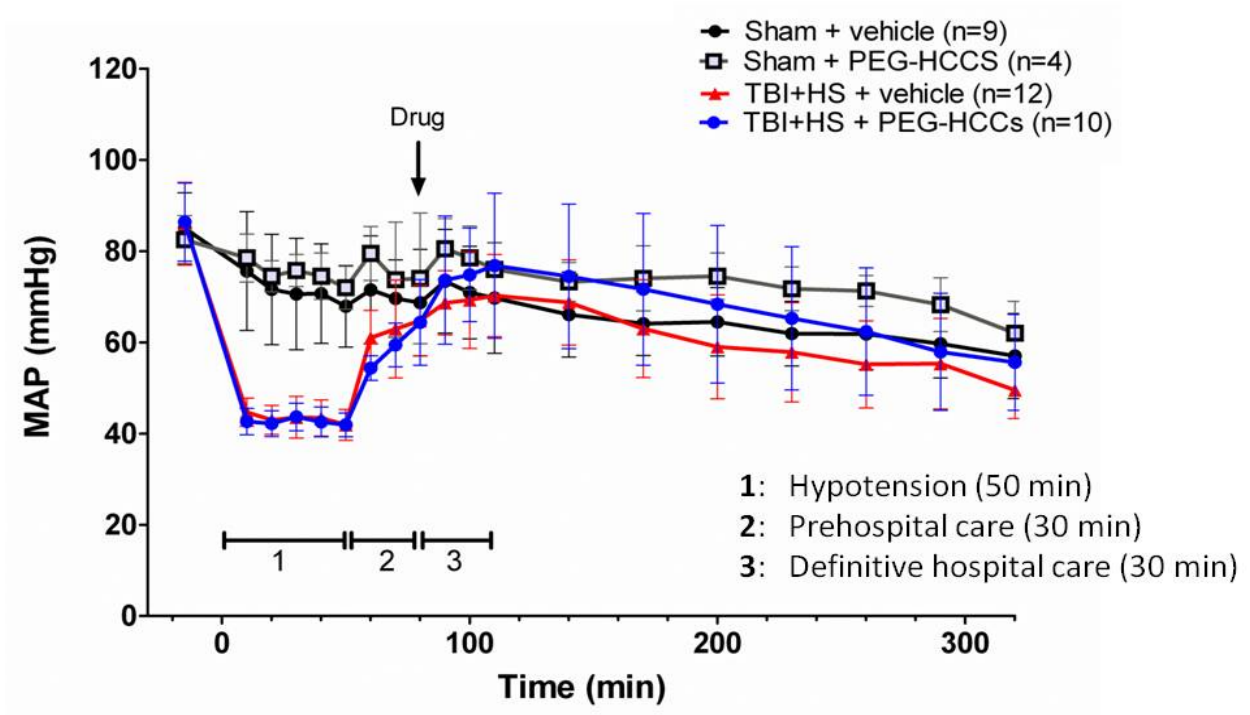


Figure S7. MAP for rats undergoing sham surgery or TBI and hemorrhagic shock (TBI + HS). Drugs (PEG-HCC or PBS vehicle) were given where indicated. Time 0 min indicates when the TBI was performed. Phase 1 = TBI + hypotension; Phase 2 = PBS during “prehospital-ambulance phase”; Phase 3 = blood reinfusion during “definitive-hospital phase”. No statistical differences (p -value >0.05) seen with data calculated with repeated measures; ANOVA with Bonferroni post-test. Error bars are s.e.m.

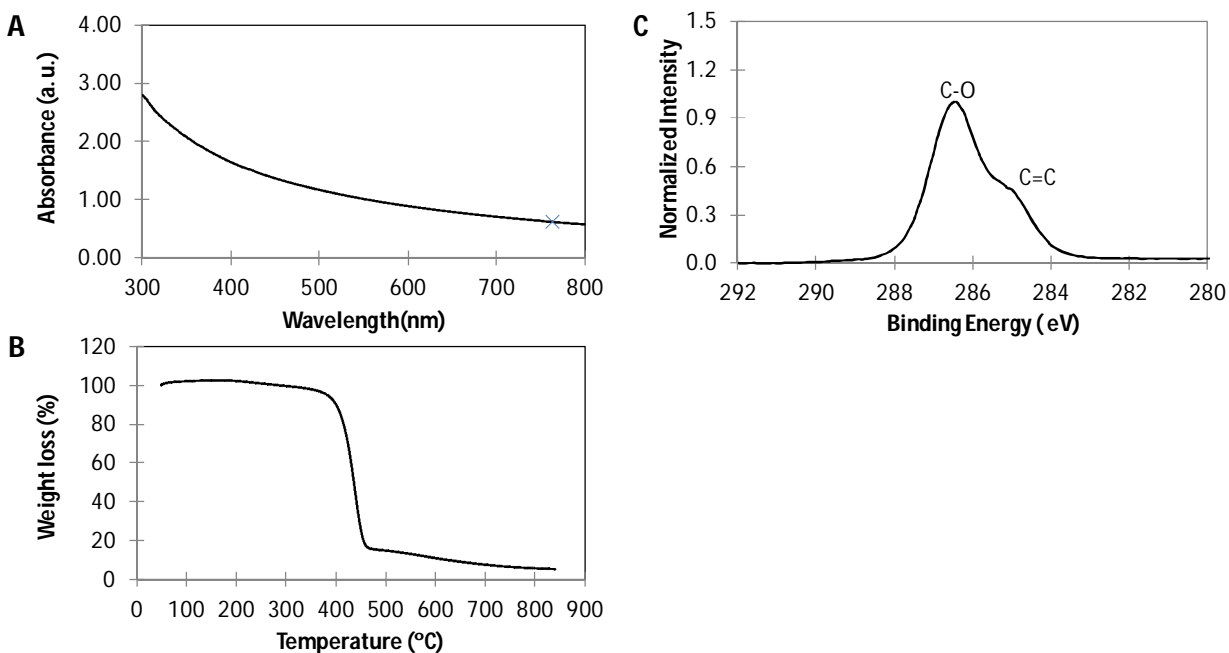


Figure S8. Characterization of the PEG-HCCs. (A) UV- spectrum of the PEG-HCCs in water. Concentration of the particles is estimated based on the carbon core absorbance at 763 nm using $\epsilon = 0.01040 \text{ mL}/\mu\text{g}$ (indicated with a X). This wavelength is not used for biological assays. (B) TGA shows a 95% weight loss (50 – 850 °C at 10 °C/min rate under Ar). The pronounced weight loss around 400 °C (84%) corresponds to the C-O functionalities of the PEG. (C) XPS spectrum of C(1s) reflects the signal corresponding to C=C at 284.5 eV as well as the strong signal corresponding to the C-O functionalization at 286.0 eV related to the PEG chains.

Supplementary Tables

Table S1. TBI impact characteristics and rat weights

Mean \pm SD	Vehicle	PEG-HCCs	p -value
Rat weight (grams)	287.1 \pm 27.0	279.0 \pm 16.0	0.3955

Impact characteristics

Velocity	m/s	3.29 ± 0.41	3.25 ± 0.49	0.8388
Duration	ms	79.0 ± 8.9	80.8 ± 5.7	0.5733

Statistics: Repeated measures ANOVA

Table S2. Arterial blood gases in the TBI and hypotension model at baseline, end of hypotension and during the hospital phase.

Arterial blood gases (mean ± SD)		Vehicle	PEG-HCCs	p -value
Baseline	pH	7.44 ± 0.06	7.45 ± 0.07	0.775
	pCO ₂	41.46 ± 4.07	39.08 ± 7.4	0.8425
	pO ₂	300.9 ± 80.7	309.5 ± 87.6	0.9144
Hypotension	pH	7.39 ± 0.01	7.30 ± 0.05	
	pCO ₂	41.85 ± 1.06	47.83 ± 4.99	
	pO ₂	139.1 ± 48.7	101.2 ± 36.4	
Hospital	pH	7.29 ± 0.11	7.40 ± 0.09	
	pCO ₂	41.77 ± 1.99	37.73 ± 9.44	
	pO ₂	249.9 ± 100.3	295.9 ± 85.7	

pCO₂ is the partial pressure of CO₂

pO₂ is the partial pressure of O₂

Statistics: Repeated measures ANOVA